S. Afr. J. Chem., 2024, 78, 15–23
https://journals.co.za/content/journal/chem/

DFT investigation of the structural and spectral properties of cryptolepine: an antimalarial alkaloid

El Hadji Mamadou Fall[1], Ali Zaidi[2,*], Safa Ben Amara[2], Mohamed Abdellahi Ami[2], Ndeye Arame Boye Faye[1], Thorsten Koslowski[3]

[1]*ITNA Institut, University of Cheikh Anta Diop, Dakar, Sénégal*
[2]*Laboratoire de Spectroscopie Atomique Moléculaire et Applications, Université de Tunis El Manar Faculté des Sciences de Tunis, El Manar Tunis, Tunisia*
[3]*Institut für Physikalische Chemie, Universität Freiburg, Freiburg im Breisgau, Germany*

ABSTRACT

We report a quantum chemical study of cryptolepine, an alkaloid that is of considerable pharmacological interest. We focus on solvent effects, spectroscopic properties and on chemical reactivity descriptors, such as electronegativity, hardness, and electrophilicity. On the density functional level, gas phase ^{1}H and ^{13}C nuclear magnetic resonance chemical shifts and infrared spectra agree well with experiments, although the dipole moment increases significantly with an increasing polarity of the solvent. We characterize normal modes using a potential energy distribution scheme. In the gas phase and in solution, the UV-Vis spectra are computed using time-dependent density functional theory. Here, major discrepancies between experiment and theory can only be observed in the visible range.

KEYWORDS

DFT, cryptolepine, molecular structure, spectroscopy, solvent effect

Received 24 April 2023, revised 15 September 2023, accepted 23 September 2023

INTRODUCTION

Cryptolepis sanguinolenta (Lindl.) Schtr. (Periplocaceae) is a plant used in Central and West African traditional medicine to treat malaria, diarrhea, hypertension and infectious and respiratory diseases.[1-3] This tropical plant has been the subject of research for decades, leading to the identification of many pharmacologically active compounds, such as the indoloquinoline alkaloids. The cryptolepine molecule is the main bioactive alkaloid isolated from the root bark of *C. sanguinolenta*.[4] In 1906, cryptolepine was synthesized by Fichter et al.[5] Twenty-three years later, cryptolepine was isolated by Clinquart[6] from the roots of *Cryptolepis triangularis* collected in Kisantu, in the Belgian Congo. Subsequently, this molecule was extracted by Delvaux from the same plant material.[7] In 1951, cryptolepine was extracted from a root sample of *C. sanguinolenta* in Nigeria by Gellert et al.,[8] and it has also isolated from a Ghanaian sample by Ablordeppey et al.[9] Furthermore, cryptolepine is found to be the major alkaloid constituent of the *Sida acuta* medicinal plant from Sri Lanka,[10] its pharmacological properties are mainly related to the alkaloid. Cryptolepine has also been isolated from other natural plants, namely *Justicia betonica*,[11] *J. secunda*,[12] and *Sida rhombifolia*.[13]

In addition to its isolation from natural plants, the title compound has been the target of synthetic chemistry, and its wide spectrum of biological and pharmacological properties has been investigated.[14] Its antimalarial (as a drug to treat the malaria disease) and antiplasmodial (as a substance that can inhibit the development of *Plasmodium* parasites) activities are well established either *in vivo* or *in vitro*.[15] Moreover, it is found that cryptolepine acts as an anti-inflammatory, hypotensive, antipyretic, renal vasodilator, anti-thrombotic, anti-hyperglycemic, anti-cancer,[16-17] anti-bacterial[18] and anti-diarrheal substance.[19] Cryptolepine has an anti-asthma effect,[20] and it inhibits the two principal proteases of SARS-CoV-2.[21]

The following spectroscopic data are available for cryptolepine. Experimental proton and carbon NMR assignments for cryptolepine have been published by Tackie et al.,[22] by Ablordeppey et al.,[9] and by Cimanga et al.[23] In the UV-Vis region, the spectrum of cryptolepine was observed in ethanol and 1,4-dioxane, and a blue shift for the absorption band was found in polar solvents.[24]

However, to the best of our knowledge, there are no theoretical studies on cryptolepine. The present work aims at investigating the electronic structure and the spectral properties of this naturally occurring alkaloid in detail. This study is dedicated to the isolated molecule, and it is considered as a preliminary step to be followed by the investigation of the cryptolepine-DNA intercalations. To identify the differences between the intercalated system on the one hand and the isolated DNA and cryptolepine, on the other hand, we first have to understand each constituent and check whether theory gives the correct results. While there is a considerable amount of work on nucleases and DNA, the present paper is the first theoretical study on cryptolepine.

Our work is organized in the following way. We give a short overview of the methods employed here, and we discuss the molecular structure of the cryptolepine molecule and its reactivity. The following part addresses a theoretical spectroscopic study including IR, UV-Vis, and NMR techniques. Finally, our results are discussed and compared to experiment.

COMPUTATIONAL DETAILS

Calculations of the molecular properties of cryptolepine have been carried out using density functional theory (DFT), as implemented in the Gaussian 09 program suite.[25] The results have been visualized using the *GaussView* 6 program.[26] Geometry optimizations have been performed in the gas phase at the B3LYP level of theory,[27-28] combined with the 6-311++G(d,p) basis set.[29] To verify the stationary points and to confirm the stability of the optimized geometries, harmonic vibrational frequencies have been calculated from the second derivatives of the energy. Positive values of all computed vibrational wavenumbers ensure that the optimized geometry is located at a true local minimum on the potential energy surface.

Furthermore, chemical reactivity descriptors of cryptolepine, such as the hardness (η), the electronegativity (χ) and the electric dipole moment have been computed in the gas phase and in solution. The descriptors (χ) and (η) can be expressed as the first and the second derivatives of the total electronic energy with respect to the number

*To whom correspondence should be addressed
Email: ali.zaidi@ipest.rnu.tn

ISSN 1996-840X Online / South African Chemical Institute / http://saci.co.za/journal

https://doi.org/10.17159/0379-4350/2024/v78a03

N of electrons at fixed external potential Vex, $\chi = -\left(\frac{\partial E}{\partial N}\right)_{V_\alpha}$ and $\eta = \left(\frac{\partial^2 E}{\partial N^2}\right)_{V_\alpha}$, respectively.[30]

Based on a standard finite difference formula, and considering molecular orbital theory, the electronegativity, and hardness are given by: $\chi = -\frac{1}{2}(E_{LUMO} + E_{HOMO})$ and $\eta = E_{LUMO} - E_{HOMO}$. Here, HOMO and LUMO refer to the Highest Occupied Molecule Orbital and Lowest Unoccupied Molecule Orbital, respectively. To characterize the molecular reactivity of the cryptolepine molecule, we also calculate the global electrophilicity index by $\omega = \frac{\chi^2}{2\eta} = \frac{(E_{LUMO} + E_{HOMO})^2}{8(E_{LUMO} - E_{HOMO})}$.[31] The electrophilicity of a molecule measures its reactivity towards the attraction of electrons from a nucleophile. As the formula indicates, a high χ value and a low η value are characteristic of a strongly electrophilic compound.

The same level of theory was applied to simulate IR, NMR, and the UV-Vis spectra of the title molecule in the gas phase, using the optimized geometries. The vibrational analysis and the vibrational mode assignments are based on the potential energy distribution (PED), they have been performed using the Vibrational Energy Distribution Analysis VEDA-4 program.[32] To be comparable to experimental results, the calculated harmonic frequencies are scaled using a factor value of 0.967.[33] The Gauge Independent Atomic Orbitals (GIAO) theory[34] has been applied to compute the ^{1}H and ^{13}C NMR chemical shifts. These calculations are again based on optimized geometries, as described above. While gas phase computations can only be an approximation to a more complex situation occurring in solution, their applicability will be shown in the Results and Discussion for the molecule under review.

In addition, the UV-Vis spectra have been computed using the time-dependent DFT (TD-DFT) method.[35] The Molecular Electrostatic Potential (MEP) and the (HOMO) and (LUMO) frontier molecular orbitals have also been investigated to analyze electronic transitions in cryptolepine.

RESULTS AND DISCUSSION

Molecular geometry

The geometry optimization has been performed at the DFT-B3LYP/6-311++G(d,p) level of theory. For the converged geometry, we find a total energy of -726.606 a.u. The optimized bond lengths and bond angles of cryptolepine are listed in Table 1 and compared with experimental data.[36] As cryptolepine has not been crystallized yet,[37] we have taken the experimental results from the hydrochloride salt of the compound.[36] The molecular structure, along with the enumeration of the atoms is plotted in Figure 1 using the output of the Gaussian 09 and *GaussView* 06 programs. The molecule can be interpreted as the fused structure of two indole (rings C and D) and two quinoline (rings A and B) moieties. The cryptolepine molecule is slightly bent, with a dihedral angle C6'C5N5C5' of 6.2°, these atoms bridge the B and C aromatic rings. The computed value is in good agreement with the experimental angle of 6.8°.[38] The small deviation from planarity is due to the five-membered ring located between the two aromatic groups, which induces an asymmetric structural element.

Table 1. Internal coordinates of the cryptolepine molecule in the gas phase.

Bond length (Å)			Bond angle (°)		
Ring A	Calculated	Experiment[36]	Ring A	Calculated	Experiment[36]
C1-C2	1.373	1.367(5)	C1-C2-C3	119.5	119.3(3)
C2-C3	1.409	1.408(5)	C2-C3-C4	120.8	121.2(3)
C3-C4	1.379	1.377(5)	C3-C4-C4'	120.6	120.2(3)
C4-C4'	1.414	1.403(5)	C4-C4'-C1'	119.0	119.4(3)
C1'-C4'	1.433	1.430(5)	C4'-C1'-C1	118.3	118.3(3)
C1'-C1	1.420	1.414(5)	C1'-C1-C2	121.7	121.7(3)
Ring B			Ring B		
C4'-N5	1.387	1.399(4)	C1'-C4'-N5	119.2	119.4(3)
N5-C5	1.363	1.348(4)	C4'-N5-C5	120.8	120.5(3)
C5-C11'	1.467	1.434(4)	N5-C5-C11'	120.7	120.1(3)
C11'-C11	1.377	1.375(5)	C5-C11'-C11	118.8	120.1(3)
C11-C1'	1.413	1.401(5)	C11'-C11-C1'	119.8	118.6(3)
			C4'-C1'-C11	120.4	120.2(3)
Ring C			Ring C		
N5-C5'	1.467	-	C5-C6'-C10	103.2	104.7(3)
C5-C6'	1.411	1.433(5)	C6'-C10-N10	114.4	110.0(3)
C6'-C10	1.456	1.431(5)	C10-N10-C11'	104.5	109.3(3)
C10-N10	1.351	1.376(5)	N10-C11'-C5	112.3	108.3(3)
N10-C11'	1.352	1.363(5)	C11'-C5-C6'	105.5	107.3(3)
Ring D			Ring D		
C6'-C6	1.420	1.421(5)	C6'-C6-C7	119.3	119.1(3)
C6-C7	1.375	1.369(5)	C6-C7-C8	120.9	122.0(3)
C7-C8	1.423	1.402(5)	C7-C8-C9	121.7	120.9(3)
C8-C9	1.374	1.381(5)	C8-C9-C10	119.2	118.0(3)
C9-C10	1.417	1.394(5)	C9-C10-C6'	119.3	122.1(3)
			C10-C6'-C6	119.6	117.8(3)

S. Afr. J. Chem., 2024, 78, 15–23
https://journals.co.za/content/journal/chem/

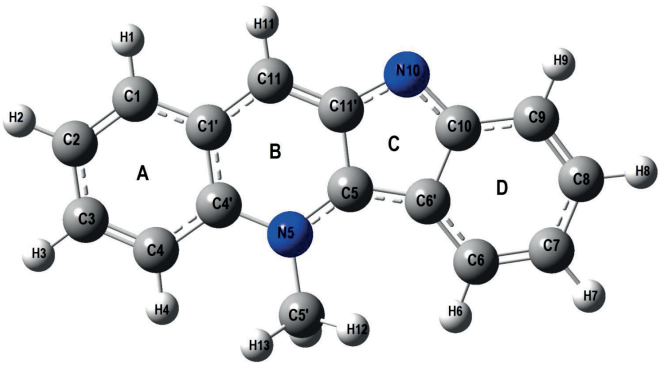

Figure 1. Optimized structure of cryptolepine.

As is shown in Figure 1, cryptolepine has an almost planar structure, and the bond lengths in the four rings vary from 1.351 Å to 1.467 Å with an average value of 1.404 Å. The standard deviation of the calculated bond lengths (0.033 Å) is in good agreement with the experimental one (0.026 Å). The maximum bond length was calculated for C5-C11' (1.467 Å), and corresponds to the observed C5-C6' bond length of 1.433 Å. The minimum bond length corresponds to C10-N10 (1.351Å) and agrees well with the experimental value. The average hetero-nuclei bond length (1.391Å) is slightly smaller than the homo-nuclei bond (1.410 Å). The bond angles in A, B and D rings have an average value of 120°, while the CCC bond angle amounts to 107.9°. These values are in good agreement with the experimental values of 120° and 108.0°, respectively. The slight difference between experimental and theoretical values can be explained by the fact that the theoretical values are obtained in the gas phase and the experimental ones in the solid phase. In addition, intramolecular interactions play a role in the crystalline structure. Despite these small differences that may be due to factors such as packing effects and the presence of a counterion in the solid phase, the calculated geometrical parameters represent a good approximation that we can rely on in subsequent calculations, such as the computation of vibrational frequencies, nuclear magnetic resonance parameters, and UV-Vis spectra.

Molecular reactivity and solvent effects

Understanding the reactivity of drugs is very useful to investigate fundamental biological processes. In particular, the chemical reactions of alkaloid derivatives, including cryptolepine, have been extensively studied.[1-5] It was found that cryptolepine interacts with DNA in the manner of a pi-stacking intercalation,[38] and that the positively charged cryptolepine acts as an electrophile. It is located in a position where the negative electrostatic potential of the DNA exhibits a maximum.

The molecular electrostatic potential is very useful to analyze electrostatic interactions between a molecule and its environment, and thus can help to predict its chemical reactivity. To understand the cryptolepine chemical reactivity, we have computed its Molecular Electrostatic Potential Surface (MEPS), again at the B3LYP/6-311++G(d,p) level of theory. The resulting MEPS is shown in Figure 2, where it is mapped onto the molecular electron density with an isodensity surface value of 0.002 a.u. Figure 2 provides a visual representation of the chemically active sites. The relative reactivity of the atoms is represented by their colour: negative and positive electrostatic potentials are shown in red and blue, respectively, while areas with a potential close to zero are shown in green.

As can be seen from Figure 2, the region with a negative potential is located around the N10 atom of the indoline moiety, reflecting the effect of the nitrogen lone pair, whereas the positive region of the MEPS covers the N5-CH_3 group of the quinoline moiety. The N10 and N5 nitrogen atoms induce asymmetry to the molecule, and this fact explains the direction of the electric dipole moment of cryptolepine. The molecule contains an electrophilic site around the N5-CH_3 group and a nucleophilic region near the nitrogen N10 atom. Consequently,

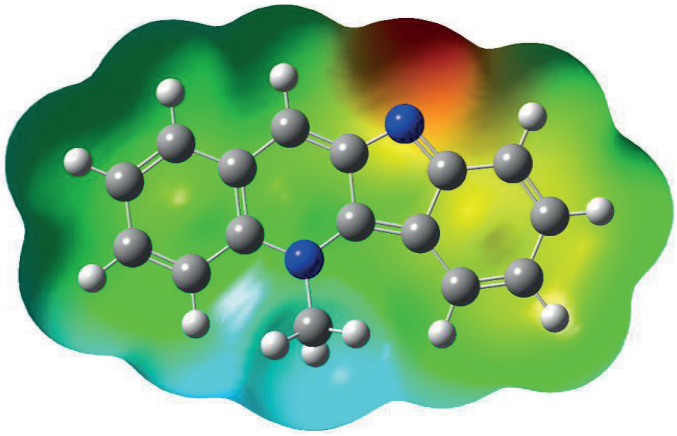

Figure 2. Molecular electrostatic potential surface.

cryptolepine can act as an electrophile or as a nucleophile with respect to its biological activity, and the most probable regions for electrophilic or nucleophilic attack are located around the nitrogen atoms.

In previous studies,[38] it was found that cryptolepine binds to DNA in a noncovalent intercalating manner. This is consistent with the nearly planar structure computed here, which enables stacking between successive DNA base pairs.[39] From the HOMO and LUMO molecular orbitals displayed in Figure 7, we can deduce that this stacking is probably stabilized by π-π interaction between cryptolepine and DNA bases. Indeed, the stability of the cryptolepine-DNA intercalation complex is enhanced by the asymmetric structure of cryptolepine, which leads to strong stacking with DNA asymmetric sites.[40]

The chemical hardness (η), electronegativity (χ) and electrophilicity (ω) of cryptolepine have been computed in terms of the one-electron energies E_{HOMO} and E_{LUMO} of the frontier molecular orbitals using the equations given in section 2. The B3LYP method and the 6–311++G(d,p) basis set have been employed to calculate η, χ and ω global reactivity descriptors and electric dipole moment in the gas phase.

To investigate solvent effects on the molecular structure, additional calculations at the same level of theory have been performed based on the polarizable continuum model (PCM). Classical solvents in chemical laboratory with different dielectric constant have been selected: chloroform (ε = 4.7), DMSO (ε = 47) and water (ε = 78).

The results are summarized in Table 2, where we can see that the cryptolepine molecule has a large electric dipole moment and exhibits a noticeable increase with increasing solvent polarity from 5.76 D in the gas phase to 8.87 D in water. In addition, electronegativity and hardness exhibit the opposite trend when moving from the vacuum to solution. The electronegativity increases with increasing solvent polarity, whereas the resistance to charge transfer measured by η decreases and, thus, the softness of the molecule increases.

According to an electrophilicity scale of organic molecules,[41] cryptolepine can be considered as a moderate electrophile, since its electrophilicity takes the value of 1.45 eV in vacuum and lies in the range of $0.8 < \omega < 1.5$ eV. The electrophilicity is slightly dependent on

Table 2. Medium effect on E_{HOMO}, E_{LUMO}, hardness, electronegativity, electrophilicity, dipole moment and Gibbs free energy of solvation ($\Delta G_{solvation}$). $\Delta G_{solvation}$ in kcal mol^{-1} and other values in eV.

	Gas	Chloroform	DMSO	Water
E_{HOMO}	-5.17	-5.35	-5.44	-5.45
E_{LUMO}	-2.52	-2.56	-2.60	-2.60
Electronegativity	3.85	3.96	4.02	4.03
Hardness	2.65	2.78	2.84	2.85
Electrophilicity	2.80	2.82	2.84	2.85
Dipole moment	5.76	7.83	8.81	8.87
$\Delta G_{solvation}$	-	-6,34	-9.40	-9.58

the medium since its magnitude changes from 1.45 eV in the gas phase to 1.42 eV in water. Furthermore, the Gibbs free energy of solvation of the title compound was calculated, and the corresponding results are given in Table 2. All computed values are negative, which implies that solvation always is an exergonic process.

Spectroscopic data

In this section, computations of the IR, NMR and UV-Vis spectra of cryptolepine are presented. The calculations have been performed at the B3LYP/6-311++G(d,p) level of theory, using the optimized geometries as described above.

Infrared spectroscopy

As shown in Figure 1, the cryptolepine molecule is a tetracyclic hetero-aromatic compound with a methyl group at the N5 nitrogen atom. It includes 30 atoms, 33 bonds and exhibits 84 nonzero vibrational modes. Based on the geometry of the ground state described and discussed in section III-1, the corresponding infrared spectrum was computed using the standard procedure of the Gaussian 09 program[25] at the B3LYP/6-311++G(d,p) level of theory. IR calculations using the B3LYP method usually overestimate the fundamental normal modes, and a rescaling factor very close to unity is commonly used for the wavenumbers.[33] In our calculations, the theoretical wavenumbers have been rescaled with a factor of 0.967. Figure 3 displays a comparison between the rescaled spectrum of cryptolepine and the observed spectrum,[42] which is conveniently presented in transmission. A Lorentzian function with a half-width of 4 cm^{-1} has been used to broaden all computed lines. Our results show an excellent agreement with experiments through the wavenumbers range accessible by standard equipment, as shown in the correlation graph of experimental and theoretical FT-IR spectra depicted in Figure 4.

Indeed, the corresponding correlation coefficient is R^2 = 0.9995. The calculated and scaled vibrational wave numbers are listed in Table 3 and are compared to the experimental results. Vibrational analysis and vibrational mode assignments of the different IR modes are based on the potential energy distribution (PED) scheme and have been performed using the VEDA 4 program.[32] We note that the VEDA program only allows the identification of types of vibrations and the contributing elements, but there is no straightforward way of identifying the atomic numbers. A detailed description of the main harmonic modes is presented in the following sections.

Aromatic C-C vibrations

The FT-IR C-C stretching modes in aromatic compounds show strong vibrational bands usually located in the 1600 –1400 cm^{-1} wavenumber range. The calculated and scaled C-C stretching modes are obtained at 1617, 1593, 1570, and 1518 cm^{-1}, and they agree rather well with the experimental values observed at 1638, 1615, 1580, 1507 cm^{-1}.[42] Other calculated IR bands have been computed at 1369, 1289, and 1019 cm^{-1}, and the corresponding experimental bands are observed at 1369, 1290, and 1040 cm^{-1}. Calculated and experimental wavenumbers slightly disagree since measurements have been done in solution, whereas our calculations are performed for an isolated molecule. Additional IR bands are calculated at 1533, 1325, 1109 cm^{-1}, and assigned to C-C vibrational stretching modes, and no corresponding observed bands are reported.

Aromatic and five-membered rings show CCC in-plane and CCCC out-of-plane bending vibrations. Planar deformations of benzene rings give rise to the in-plane bending modes calculated at 997, 976, 866, 857, 779, 663, 583, and 548 cm^{-1}, in good agreement with the observed modes at 989, 883, 846, 793 and 664 cm^{-1}. The calculated CCCC out of plane vibrational modes lie at 737, 555, 413, 303, 223, 166, 83 and 57 cm^{-1}, and the observed IR spectrum exhibits only one corresponding band at 753 cm^{-1}.

C-N vibrations

C-N stretching vibrational modes are difficult to identify since they occur in a mixture with other modes.[43] Silverstein et al. found that C-N vibration modes in heteroaromatic nitrogen compounds lie in the region of 1382-1266 cm^{-1}. In our work, we observe these bands at 1311, 1289, 1272, 1256, 1229 and 1016 cm^{-1}, with a major contribution of the PED equals 25%. The experimental spectrum shows three C-N stretching modes at 1290, 1259, and 1219 cm^{-1}. Moreover, the nitrogen N atom involved in ring skeleton deformations leads to numerous bending modes including the CNC and CCN in-plane or out-of-plane modes and the CCCN and CCNC torsion and out-of-plane modes. The former vibrational modes are calculated at 866, 823, 737, 692, 471, 447, 413, 328, 223, 166, 116, 83, 57 cm^{-1}, while the latter ones lie at 711, 621, 583, 548, 529, 483, 373, 366, 314, 186 cm^{-1}. For these bending vibrations, very few experimental data are observed and only two bending modes are found at 883 cm^{-1} and 753 cm^{-1}. They can be assigned to the in-plane NCC and to the out-of-plane CCNC bending modes, respectively.

C-H vibrations

The cryptolepine molecule contains a $-CH_3$ methyl group attached to the nitrogen atom at position N5. This gives rise to symmetric and asymmetric C-H stretching modes with well-defined peaks lying at 2948 cm^{-1} and 3034 cm^{-1}, respectively. These features have been detected in absorption at 2922 cm^{-1}.[42] The aromatic CH moieties of the four rings show different stretching modes with a weak-to-moderate band

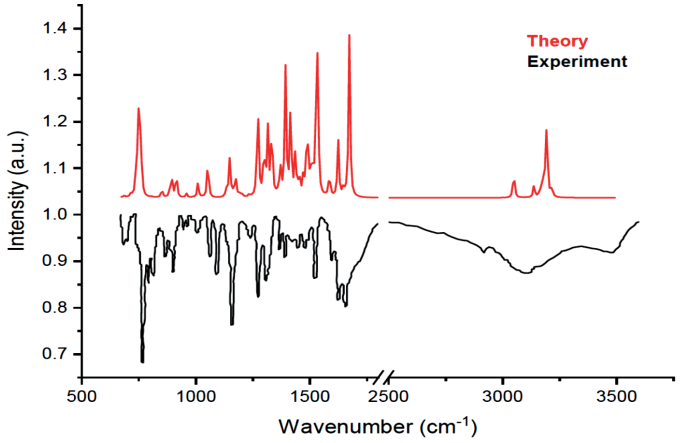

Figure 3. Observed and simulated IR spectra.

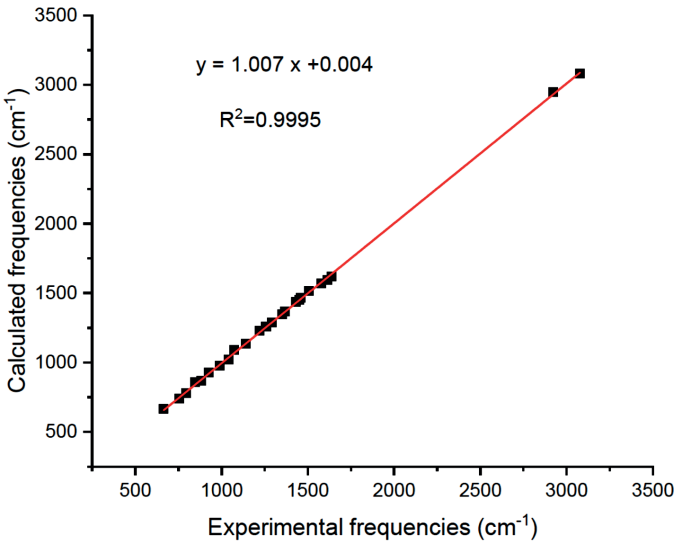

Figure 4. Theoretical versus experimental IR frequencies.

Table 3. IR wavenumbers and vibrational modes assignments.

Mode	Scaled		Experiment[42]	Vibrational Assignments (%PED)
84	3216	3110	-	υCH(91)
83	3195	3089	-	υCH(28) + υCH(22) + υCH(10) + υCH(27)
82	3194	3089	-	υCH(13) + υCH(59) + υCH(14)
81	3190	3085	-	υCH(56) + υCH(28)
80	3184	3079	3078	υCH(94)
79	3179	3074	-	υCH(56) + υCH(24)
78	3178	3073	-	υCH(23) + υCH(34) + υCH(12)
77	3171	3066	-	υCH(20) + υCH(38) + υCH(12)
76	3170	3065	-	υCH(47) + υCH(25) + υCH(13)
75	3161	3057	-	υCH(23) + υCH(65)
74	3137	3034	-	υCH(13) + υCH(65) + υCH (20)
73	3049	2948	2922	υCH(13) + υCH(78)
72	1673	1617	1638	υCC(15) + υCC(23) + υCC(12)
71	1647	1593	1615	υCC(17) + υCC(17) + υCC(10) + υCC(11) + βHCC(11)
70	1624	1570	1580	υCC(14) + υCC(18) + υCC(15)
69	1585	1533	-	υCC(11) + υCC(10) + υNC(15)
68	1570	1518	1508	--
67	1534	1483	-	υCC(12)
66	1527	1477	-	βHCH(19)
65	1514	1464	1458	βHCH(20) + βHCH(38) + τHCNC(11)
64	1502	1453	1450	βHCH(28) + βHCH(30) + τHCNC(11)
63	1488	1439	1430	βHCC(11) + βHCC(14)
62	1472	1423	-	βHCC(12) + βHCH(25) + βHCH(11)
61	1453	1405	-	βHCC(19) + βHCC(11) + βHCC(10)
60	1437	1389	-	υNC(14) + βHCC(11) + βHCC(16)
59	1416	1369	1369	υCC(16) + βHCC(11)
58	1393	1347	1353	--
57	1370	1325	-	υCC(12) + υCC(13) + βHCC(15)
56	1356	1311	-	υNC(11)
55	1333	1289	1290	υCC(10) + υNC(10)
54	1315	1272	-	υNC(10) + βCNC(12)
53	1299	1256	1259	υNC(25) + βHCC(11)
52	1272	1229	1220	υNC(11) + βHCC(10) + βHCC(10) + βHCC(12)
51	1233	1193	-	βHCC(23) + βHCC(11)
50	1201	1161	-	βHCC(10) + βHCC(35) +βHCC (12) + βHCC (12)
49	1188	1149	-	βHCC(14)
48	1174	1135	1140	βHCC(14) + βHCC(24) + βHCC(13)
47	1159	1120	-	βHCH(10) + τHCNC(12) + τHCNC(21)
46	1148	1109	-	υCC(15) + βHCC(21) + βHCC(16)
45	1135	1098	-	βHCH(19) + τHCNC(40) + τHCNC(17)
44	1128	1091	1075	---
43	1054	1019	1041	υCC(38)
42	1051	1016	-	υNC(24) + βCCC(11)
41	1031	997	-	βCCC(11) + βCCC(21)
40	1009	976	989	βCCC(13)
39	986	953	-	τHCCC(24) + τHCCC(45) + τHCCC(19)
38	984	951	-	τHCCC(46) + τHCCC(31) + τCCCC(14)
37	958	926	925	τHCCC(24) + τHCCC(38) + τHCCN(30)
36	945	914	-	τHCCC(42) + τHCCC(36)

Table 3. (cont.)

Mode	Scaled		Experiment[42]	Vibrational Assignments (%PED)
35	914	884	-	τHCCC(71)
34	895	866	883	βCCC(12) + βNCC(14)
33	886	857	846	βCCC(16) + βCCC(11) + βCCC(13)
32	851	823	-	τHCCC(13) + τHCCC(16) + τHCCC(18) + ωCCNC(13)
31	849	821	793	τHCCC(18) + τHCCC(11) + τHCCN(26)
30	805	779	772	υCC(17) + βCCC(10)
29	762	737	753	τCCCC(20) + τCNCC(15) + ωCCNC(15)
28	757	732	-	τHCCC(17) + τHCCC(21) + τHCCC(23) + τHCCN(14)
27	749	725	-	τHCCN(10) + τHCCC(11) + τHCCC(15)
26	744	719	-	τHCCC(11) + τHCCC(20) + τHCCC(12)
25	735	711	-	υCC(10) + βCCC(13) + βCNC(27)
24	715	692	-	τCNCC(12) + ωCNCC(14) + ωNCCC(23)
23	686	663	664	βCCC(10) + βCCC(18) + βCCC(16)
22	642	621	-	βCCN(13)
21	603	583	-	υCC(10) + βCCN(12) + βCCC(10) + βCCC(12)
20	574	555	-	τCCCC(12) + τCCCC(11) + τ CCCC(10) + τ CCCC(10)
19	567	548	-	βCCC(13) + βCCC(12) + βNCC(12) +βCCC(11)
18	558	539	-	τCCCC(14) + τCCCC(13) + τCCCC(11) + τCCCC(13) + ωNCCC(12)
17	547	529	-	υCC(10) + βCNC(10)
16	499	483	-	βCCC(13) + βCCN(10) + βNCC(11)
15	487	471	-	ωCCCN(23) + ωNCCC(13)
14	462	447	-	τHCCC(10) + ωCCCC(26) + ωCCNC(13)
13	427	413	-	τCCCC(13) + ωCCCN (12) + ωCCCC(20)
12	386	373	-	βCNC(46)
11	378	366	-	βNCC(18)
10	339	328	-	τCNCC(15) + τCCCC(14)
9	325	314	-	υCC(12) + βCNC(18)
8	314	303	-	τCCCC(13) + τCCCC(13) + τCCCC(10)
7	230	223	-	τCCCC(17) + ωNCCC(11)
6	192	186	-	βNCC(16)
5	172	166	-	τCCCC(10) + ωCCNC(10) + ωNCCC(11)
4	119	116	-	τCNCC(16) + ωCCCN(26) + ωNCCC(14)
3	115	111	-	τCCCC(12) + τHCNC(22)
2	86	83	-	τCCCC(12) + τCNCC(18) + ωCCCC(14)
1	59	57	-	τCCCC(14) + τCNCC (13) + τCNCC(13) + ωCCNC(11) + ωNCCC 18

υ: stretching, β: in plane-bonding, ω: out-plane-bonding, τ: torsion

that could be symmetric or asymmetric. The calculated frequencies range from 3057 to 3110 cm^{-1}. However, the CH stretching vibrations are observed as a weak and broad band centered at 3077 cm^{-1}, since the absorption spectrum is obtained in the solid state.

Moreover, the C-H bonds exhibit further vibration modes: scissoring of the CH_3 group occurs at 1477 and 1464 cm^{-1}, while the rocking mode appears at 1453 cm^{-1}. The experimental counterparts are observed at 1458 and 1450 cm^{-1}. Wagging of the CH_3 group leads to IR modes at 1423 and 1389 cm^{-1}. The in-plane HCC bending mode is calculated at 1439, 1405, 1369, 1347, 1311, 1256, 1229, 1193, 1161, 1149, 1135, 1109, and 1091 cm^{-1}. The corresponding experimental values are observed at 1369, 1352, 1259, 1219, 1139, and 1075 cm^{-1}. The frequencies of 953, 951, 926, 914, 884, 823, 821, 732, 725 and 719 cm^{-1} correspond to the out-of-plane bending of the CH_3 group, and the corresponding observed values are 924, 883, 846, 793, 772 and 753 cm^{-1}.

NMR spectroscopy

In addition to infrared spectroscopy, NMR investigations provide information about the molecular structure. In this work, the ^1H and ^{13}C chemical shifts for cryptolepine have been computed using the GIAO method at the B3LYP/6-311++G(d,p) level. The calculated values are collected in Table 4, and the corresponding experimental results are also reported.[9]

As shown in Figure 5a and Figure 5b for the ^1H and ^{13}C chemical shifts, the theoretical results accurately reproduce the general trends of the experimental data. The squared correlation coefficient is equal to R^2 = 0.9686 and R^2 = 0.9947 for hydrogen and carbon atoms, respectively. This accuracy enables a reliable interpretation of the obtained NMR spectroscopic data.

In the ^1H NMR spectrum, a singlet observed at 4.92 ppm indicates an equivalent behaviour of the three hydrogen atoms of the methyl group, whereas our calculations give rise to three slightly different

Table 4. Calculated ^{1}H and ^{13}C NMR data of cryptolepine.

Atom	Gas	Experiment[9]	Atom	Gas	Experiment[9]
C1	135.5	129.6	H1	8.41	8.40
C2	126.3	123.9	H2	7.70	7.69
C3	131.1	128.9	H3	7.86	7.90
C4	117.2	116.6	H4	8.08	8.53
C4'	137.6	132.8	H6	8.37	8.51
C5	145.0	139.0	H7	7.12	7.05
C6'	119.2	113.8	H8	7.67	7.53
C6	127.6	125.1	H9	8.03	7.66
C7	121.2	116.6	H11	8.87	8.95
C8	135.9	130.4	H12-14	4.75	4.92
C9	127.3	119.5			
C10	170.9	160.0			
C11'	151.9	144.4			
C11	131.7	126.2			
C1'	129.9	124.4			
C5'	37.7	38.9			

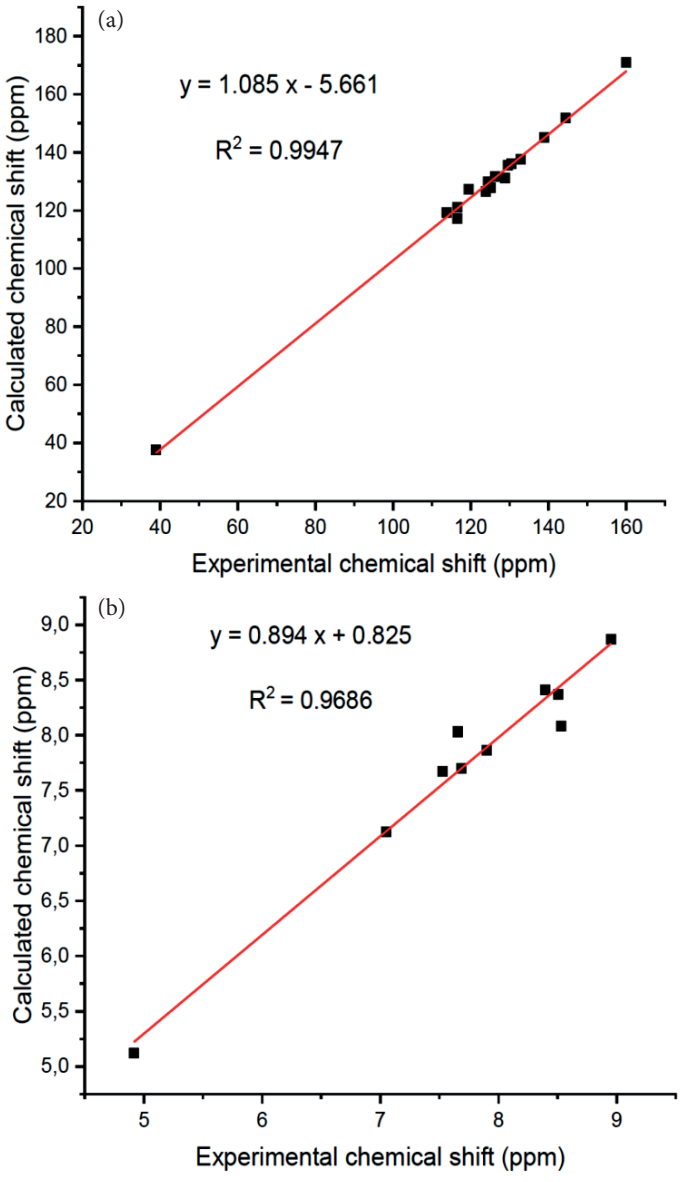

Figure 5. (a) Theoretical versus experimental ^{1}H chemical shifts. (b) Theoretical versus experimental ^{13}C chemical shifts.

values of 5.12, 4.76, and 4.36 ppm. This difference is related to the fact that the computations have been performed for a static molecule. Thus, the three hydrogen atoms are non-equivalent. However, the average NMR chemical shift of 4.75 ppm is very close to the experimentally observed value of 4.92 ppm.

The protons of the conjugated double bonds of the aromatic rings are more deshielded than those of the methyl group due to van der Waals interactions. The H2, H3, H7, and H8 hydrogen atoms are almost equivalent, and the corresponding peaks are calculated at 7.70, 7.86, 7.12, and 7.67, and observed at 7.69, 7.90, 7.05, and 7.53, respectively. H1, H4, H6, and H9 have a similar environment, and so they show nearly the same calculated chemical shifts at 8.41, 8.08, 8.37, and 8.03 ppm, respectively. H11 is the most deshielded hydrogen atom, with 8.87 ppm and 8.95 obtained theoretically and experimentally, respectively. As shown in Table 5, the calculated ^{13}C NMR chemical shifts for the cryptolepine molecule lie within the range of typical organic molecules, which is usually higher than 100 ppm.

The decrease of the charge density around the C11', C5 and C4' carbon atoms gives rise to a notable deshielding effect induced by the electronegativity of the nitrogen atom and π-electron delocalization effects. The signal attributed to the sp^3-hybridized C5' carbon atom of the methyl group appears at a chemical shift of 37.7 ppm, and it is slightly smaller than the corresponding experimental value of 38.9.

UV-Vis spectrum

Time-Dependent Density Functional Theory (TD-DFT)[35] has been used to compute the vertical transition energies at the B3LYP/6-311++G(d,p) level. The UV-Vis spectrum of cryptolepine was simulated in the gas phase and in chloroform, DMSO, and water. The 250–700 nm wavelength range has been selected to compare our calculations to experiment. In Table 5, vertical excitation energies, oscillator strengths and wavelengths of the main electronic transitions in the UV-Vis region are summarized.

The predicted UV-Vis spectra are displayed in Figure 6, where we can see two main absorption peaks at 300 and 375 nm. These values agree well with the observed peaks at 301 and 380 nm.[44] In the visible region, a very weak, broad absorption band is computed with an absorption maximum at 602 nm in the gas phase and around 550 nm in solution It can be assigned to the observed peak at 560 nm.[44] We refer to these peaks as band 1, band 2 and band 3, respectively with increasing wavelength. There may be several rotational and vibrational sublevels in the ground and excited states that attribute to the features of band 3. Figure 6 shows different solvent effects: a pronounced hypsochromic shift of ~37 nm is found in band 3 when going from the gas phase to chloroform and of 17 nm when increasing the polarity of the solvent from chloroform to DMSO. In the UV region, a smaller solvent effect is calculated in bands 1 and 2, with a hypsochromic shift in band 2 and a bathochromic one in band 1. Bands 2 and 3 show a higher absorption strength in solvent than in vacuum, while band 1 displays the opposite behaviour.

To discuss the UV-Vis spectrum and to investigate the localization and delocalization of the electron density, we present in Figure 7 a 3D plot of the main Frontiers Molecules Orbitals participating in the vertical electronic transitions. The red and green colours refer to positive and negative phases, respectively. Figure 7 shows that the HOMO and LUMO electron density are almost uniformly distributed over the entire molecule. From Table 2, we can see that in polar solvents, solute-solvent interactions reduce the energy of both the ground and excited state, but the HOMO exhibits a stronger stabilization than the LUMO. Thus, the HOMO-LUMO energy gap decreases, leading to the hypsochromic shift in band 3 displayed in Figure 6. As shown in Table 5, the electronic transition at 602 nm (2.05 eV) is dominated by the HOMO-LUMO contribution, and it can be characterized as a π-π^* transition. With the help of Figures 6 and 7, the blue shift in band 3 can be interpreted, as the HOMO has a more delocalized electron density than the LUMO. In the UV-Vis region, the maximum absorptions

Table 5. Experimental and calculated UV-Vis data of cryptolepine.

Gas			Chloroform			DMSO			Water			Experiment[44]		Major contribution
λ_{max} (nm)	*E* (eV)	*f*	λ_{max} (nm)	*E* (eV)	*f*	λ_{max} (nm)	*E* (eV)	*f*	λ_{max} (nm)	*E* (eV)	*f*	λ_{max} (nm)	*E* (eV)	
602	2.06	0.0172	565	2.19	0.0296	548	2.26	0.0313	548	2.26	0.0319	560	2.21	HOMO-LUMO
373	3.32	0.1678	371	3.34	0.3711	368	3.37	0.3791	367	3.38	0.3686	380	3.26	HOMO-1-LUMO
295	4.20	1.1144	303	4.09	0.7784	299	4.14	0.9356	298	4.16	0.9099	301	4.12	HOMO-LUMO+1

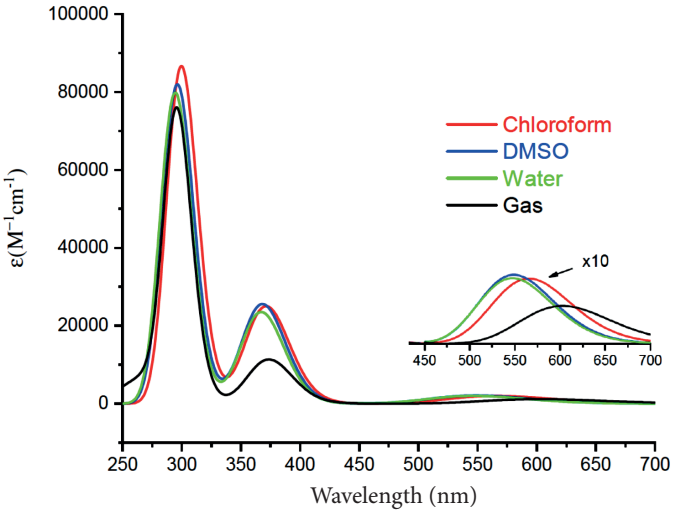

Figure 6. Simulated UV-Vis spectra in vacuum and in solution.

calculated at 300 nm and 375 correspond to HOMO → LUMO+1 and HOMO-1 → LUMO electronic transitions, respectively, and they can be assigned to π-π* transitions.

CONCLUSION

In this work, the cryptolepine molecule has been investigated theoretically at the DFT/B3LYP/6-311++G(d,p) level of theory. The calculated geometrical parameters have been compared to experimental values, and cryptolepine can be considered as a near-planar molecule. ESP computations help to rationalize its biological activity, the most probable regions involved in both electrophilic and nucleophilic attack are located around the nitrogen atoms of the molecule. The molecule has a large electric dipole moment, which increases with increasing solvent polarity. Consequently, cryptolepine is expected to be more soluble in polar than in unipolar solvents. The η, χ and ω global reactivity descriptors have been calculated in the gas phase and in solution, and the resulting solvent effects have been discussed.

The IR spectrum has been simulated, and the different vibrational modes have been assigned. The computed frequencies have been compared to the observed ones, and small discrepancies have been related to different media used in the experimental and calculated spectra. The experimental UV-Vis spectrum and the quantum chemical data computed in our work show an excellent agreement. ^{1}H and ^{13}C NMR chemical shifts of the title compound have been obtained, and discrepancies with the observed ones have been discussed. The solvent effect on the UV-Vis spectra has been investigated, and the λ_{max} values of the main observed absorption bands have been calculated successfully.

SUPPLEMENTARY MATERIAL

The input file for cryptolepine and the cartesian coordinates of its optimized structure are provided as supplementary information.

ACKNOWLEDGEMENTS

El Hadji Mamadou Fall expresses gratitude to the Abdus Salam ICTP for providing financial support for this work through the OEA-NET-05 project.

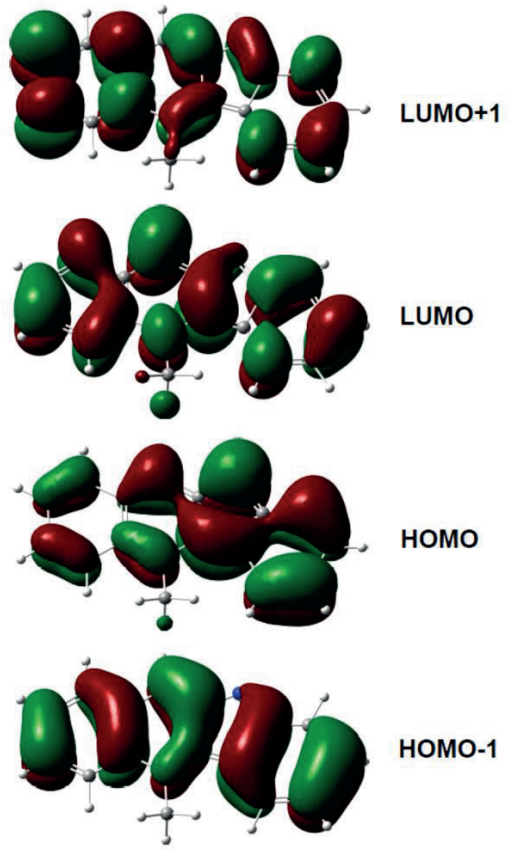

Figure 7. HOMO and LUMO 3D plots.

ORCID IDS

El Hadji Mamadou Fall: https://orcid.org/0000-0002-7007-3358
Ali Zaidi: https://orcid.org/0000-0002-5463-2252
Safa Ben Amara: https://orcid.org/0009-0003-7500-7282
Mohamed Abdellahi Ami: https://orcid.org/0000-0001-9558-0893
Ndeye Arame Boye Faye: https://orcid.org/0000-0003-3188-5051
Thorsten Koslowski: https://orcid.org/0000-0002-1844-2152

REFERENCES

1. Schwikkard S, Van Heerden RF. Anti-malarial activity of plant metabolites. Nat Prod Rep. 2002;19:675–692. https://doi.org/10.1039/B008980J
2. Zofou D, Kuete V, Titanji VPK. Antimalarial and other antiprotozoal products from African medicinal plants. In: Kuete V, ed. Medicinal Plant Research in Africa: Pharmacology and Chemistry. Oxford: Elsevier. 2013:661–709. https://doi.org/10.1016/B978-0-12-405927-6.00017-5
3. Schmidt TJ, Khalid SA, Romanha AJ, Alves TMA, Biavatti MW, Brun R, Da Costa FB, de Castro SL, Ferreira VF, de Lacerda MVG, et al. The potential of secondary metabolites from plants as drugs or leads against protozoan neglected diseases-part II. Curr Med Chem. 2012;19:2176–2228. https://doi.org/10.2174/092986712800229023
4. Osafo N, Mensah KB, Yeboah OK. Phytochemical and pharmacological review of *Cryptolepis sanguinolenta* (Lindl.) Schlechter. Adv Pharmacol Sci. 2017;2017:3026370. https://doi.org/10.1155/2017/3026370
5. Fichter F, Rohner F. Uber einige derivate des chindolins. Chem Ber. 1910;43(3):3489–3499.

6. Clinquart E. Sur la composition chimique de cryptolepis triangularis, plante congolaise. (On the chemical composition of cryptolepis triangularis, plants from the (Belgian) Congo.). Bull Acad R Med Belg. 1929;9:627–635.
7. Delvaux E. Sur la cryptolépine (on cryptolepine). J Pharm Belg. 1931;13:955–959.
8. Gellért E, Hamet R, Schlittler E. Die konstitution des alkaloids cryptolepin (the constitution of the alkaloid cryptolepine). Helv Chim Acta. 1951;34(2):642–651. https://doi.org/10.1002/hlca.19510340228
9. Ablordeppey SY, Hufford CD, Borne RF, Dwuma-Badu D. ^{1}H-NMR and ^{13}C-NMR assignments of cryptolepine, a 3:4- benz-δ-carboline derivative isolated from *Cryptolepis sanguinolenta*. Planta Medica. 1990;56(4):416–417. https://doi.org/10.1055/s-2006-960998
10. Gunatilaka AAL, Sotheeswaran S, Balasubramaniam S, Chandrasekara AL, Sriyani HTB, Studies on medicinal plants of Sri Lanka. J Planta Med. 1980;39(5):66–72. https://doi.org/10.1055/s-2008-1074904
11. Subbaraju GV, Kavitha J, Rajasekhar D, Jimenez JI. Jusbetonin, the first indolo[3,2-b] quinoline alkaloid glycoside, from justicia betonica. J Nat Prod. 2004;67(3):461–462. http://dx.doi.org/10.1021/np030392y
12. Calderón AI, Hodel A, Wolfender JL, Gupta MP, Correa M, Hostettmann K. Lc-dad-ms-based metabolite profiling of three species of Justicia (Acanthaceae). Nat Prod Res. 2013;27(15):1335–1342. https://doi.org/10.1080/14786419.2012.738207
13. Chaves OS, Teles YCF, Monteiro MMDO, Mendes Junior LDG, Agra MDF, Braga VDA, Silva TMS, Souza MDFVD. Alkaloids and phenolic compounds from sida rhombifolia L. (Malvaceae) and vasorelaxant activity of two indoquinoline alkaloids. Molecules. 2017;22(1):article 94. https://doi.org/10.3390/molecules22010094
14. Guittat L, Alberti P, Rosu F, Van Miert S, Thetiot E, Pieters L, Gabelica V, De Pauw E, Ottaviani A, Riou J-F, et al. Interactions of cryptolepine and neocryptolepine with unusual DNA structures. Biochimie. 2003;85(5):535–547. https://doi.org/10.1016/S0300-9084(03)00035-X
15. Cimanga K, De Bruyne T, Pieters L, Vlietinck AJ, Turger CA. In vitro and in vivo antiplasmodial activity of cryptolepine and related alkaloids from *Cryptolepis sanguinolenta*. J Nat Prod. 1997;60(7):688–691. https://doi.org/10.1021/np9605246
16. Ansha C, Mensah KB. A review of the anticancer potential of the antimalarial herbal *Cryptolepis sanguinolenta* and its major alkaloid cryptolepine. Ghana Med J. 2013;47:137–147.
17. Olajide OA, Ajayi AM, Wright CW. Anti-inflammatory properties of cryptolepine. Phytother Res. 2009;23(10):1421–1425. https://doi.org/10.1002/ptr.2794
18. Paulo A, Gomes ET, Steele J, Warhurst DC, Houghton PJ. Antiplasmodial activity of *Cryptolepis sanguinolenta* alkaloids from leaves and roots. J Planta Med. 2000;66(1):30–34. https://doi.org/10.1055/s-2000-11106
19. Paulo A, Pimentel M, Viegas S, Pires I, Duarte A, Cabrita J, Gomes ET. *Cryptolepis sanguinolenta* activity against diarrhoeal bacteria. J Ethnopharmacol. 1994;44(2):73–77. https://doi.org/10.1016/0378-8741(94)90071-X
20. Mensah-Kane P, Mensah KB, Antwi AO, Forkuo AD, Ansah C. Cryptolepine, the major alkaloid of *Cryptolepis sanguinolenta* (Lindl.) Schlechter (Apocynaceae), attenuates early and late-phase symptoms of asthma. Sci Afr. 2020;9:e00540. https://doi.org/10.1016/j.sciaf.2020.e00540
21. Borquaye LS, Gasu EN, Ampomah GB, Kyei LK, Amarh MA, Mensah CN, Nartey D, Commodore M, Adomako AK, Acheampong P, et al. Alkaloids from *Cryptolepis sanguinolenta* as potential inhibitors of SARS-CoV-2 viral proteins: an *in silico* study. Biomed Res Int. 2020;2020:1–14. https://doi.org/10.1155/2020/5324560
22. Tackie AN, Sharaf MH, Schiff JPL, Boye GL, Crouch RC, Martin GE. Assignment of the proton and carbon NMR spectra of the indoloquinoline alkaloid cryptolepine. J Heterocycl Chem. 1991;28(5):1429–1435. https://doi.org/10.1002/jhet.5570280540
23. Cimanga K, De Bruyne T, Lasure A, Van Poel B, Pieters L, Claeys M, Berghe DV, Kambu K, Tona L, Vlietinck A. *In vitro* biological activities of alkaloids from *Cryptolepis sanguinolenta*. J Planta Med. 1996;62(1):22–27. https://doi.org/10.1055/s-2006-957789
24. Lai TK, Chatterjee A, Banerji J, Sarkar D, Chattopadhyay N. A concise synthesis of the DNA-intercalating and antimalarial alkaloid cryptolepine and its fluorescence behaviour in solvents of different polarities. Helv Chim Acta. 2008;91(10):1975–1983.
25. Frisch MJ, Trucks GW, Schlegel HB, Scuseria GE, Robb MA, Cheeseman JR, Scalmani G, Barone V, Mennucci B, Petersson GA. Gaussian 09, Revision, A.1, Gaussian Inc. Wallingford, CT, USA; 2009.
26. Dennington R, Keith T, Millam J. GaussView, Version 5. Semichem Inc. Shawnee Mission, KS, USA; 2009.
27. Beke AD. Density-functional exchange-energy approximation with correct asymptotic behaviour. Phys Rev A. 1998;38(6):3098–3100. https://doi.org/10.1103/PhysRevA.38.3098
28. Lee C, Yang W, Parr RG. Development of the Colle-Salvetti correlation-energy formula into a functional of the electron density. Phys Rev B. 1988;37(2):785–789. https://doi.org/10.1103/PhysRevB.37.785
29. Woon DE, Dunning Jr TH. Gaussian basis sets for use in correlated molecular calculations III, the atoms aluminium through argon. J Chemical Physics. 1993;98(2):1358–1371. https://doi.org/10.1063/1.464303
30. Parr RG, Pearson RG. Absolute hardness: companion parameter to absolute electronegativity. J Am Chem Soc. 1983;105(26):7512–7516. https://doi.org/10.1021/ja00364a005
31. Parr RG, Von Szentpaly L, Liu S. Electrophilicity index. J Am Chem Soc. 1999;121(9):1922–1924. https://doi.org/10.1021/ja983494x
32. Jamróz MH. Vibrational Energy Distribution Analysis (VEDA). Spectrochim Acta A Mol Biomol Spectrosc. 2013;4:220–230. https://doi.org/10.1016/j.saa.2013.05.096
33. Alecu IM, Zheng J, Zhao Y, Truhlar DG. Computational thermochemistry: scale factors databases and scale factors for vibrational frequencies obtained from electronic model chemistry. J Chem Theory Comput. 2010;6(9):2872–2887. https://doi.org/10.1021/ct100326h
34. Wolinski K, Hinton JF, Pulay P. Efficient implementation of the Gauge-Independent Atomic Orbital Method for NMR Chemical Shift Calculations. J Am Chem Soc. 1990;112(23):8251–8260. https://doi.org/10.1021/ja00179a005
35. Cavillot V, Champagne B. Time-dependent density functional theory simulation of UV/visible absorption spectra of zirconocene catalysts. Chem Phys Lett. 2002;354(5–6):449–457. https://doi.org/10.1016/S0009-2614(02)00161-6
36. Hampson HC, Ho CY, Palmer RA, Potter BS, Helliwell M, Wright CW. Low temperature X-Ray crystallographic structure of the antiplasmodial compound 5-N-hydroxyethanequindoline hydrochloride 0.5 CH3OH. J Chem Crystallogr. 2011;41(11):1757–1762. http://dx.doi.org/10.1007/s10870-011-0169-5
37. Wright CW, Philpson JD, Lisgarten JN, Palmer RA. Structure of the tetraphenyl borate complex of the indoloquinoline alkaloid cryptolepine, J Chem Crystallogr. 1999;29(4):449–455. https://doi.org/10.1023/A:1009519211938
38. Dassonneville L, Bonjean K, De Pauw-Gillet MC, Colson P, Houssier C, Quetin-Leclercq J, Bailly C. Stimulation of topoisomerase II-mediated DNA cleavage by three DNA-intercalating plant alkaloids: cryptolepine, matadine, and serpentine. Biochemistry. 1999;38(24): 7719–7726. https://doi.org/10.1021/bi990094t
39. Bonjean K, De Pauw-Gillet MC, Defresne MP, Colson P, Houssier C, Dassonneville L, Bailly C, Greimers R, Wright C, Quetin-Leclercq J, et al. The DNA intercalating alkaloid cryptolepine interferes with topoisomerase II and inhibits primarily DNA synthesis in B16 melanoma cells. Biochemistry. 1998;37(15):5136–5146. https://doi.org/10.1021/bi972927q
40. Lisgarten JN, Coll M, Portugal J, Wright CW, Aymami J. The antimalarial and cytotoxic drug cryptolepine intercalates into DNA at cytosine-cytosine sites. Nat Struct Mol Biol. 2002;9(1):57–60. https://doi.org/10.1038/nsb729
41. Domingo LR, Aurell MJ, Pérez P, Contreras R. Quantitative characterization of the global electrophilicity power of common diene/dienophile pairs in Diels–Alder reactions. Tetrahedron. 2002;58(22):4417–4423. https://doi.org/10.1016/S0040-4020(02)00410-6
42. Ofori E. Development of a reverse-phase HPLC method for the quantification of cryptolepine in the dry roots of *Cryptolepis sanguinolenta*. PhD thesis, Kwame Nkrumah University of Science and Technology, Ghana; 2010.
43. Silverstein RM, Bassler GC. Spectrometric identification of organic compounds. J Chem Educ. 1962;39(11):546–553. https://doi.org/10.1021/ed039p546
44. Mariz IF, Pinto S, Lavrado J, Paulo A, Martinho JM, Maçôas EM. Cryptolepine and quindoline: understanding their photophysics. Phys Chem Chem Phys. 2017;19(16):10255–10263. https://doi.org/10.1039/C7CP00455A